Inorganic Chemistry

Article

pubs.acs.org/IC

Comparison of Redox Activity between 2-Aminothioether and 2-Aminothiophenol: Redox-Induced Dimerization of 2-Aminothioether via C−C Coupling

Pradip Ghosh,[†,§] Sutanuva Mandal,[†,§] Ipsita Chatterjee,[†] Tapan Kumar Mondal,[‡] and Sreebrata Goswami*[,†]

[†]Department of Inorganic Chemistry, Indian Association for the Cultivation of Science, Kolkata 700 032, India

[‡]Department of Chemistry, Jadavpur University, Kolkata, 700 032, India

Supporting Information

ABSTRACT: Three chemical reactions of two 2-aminothioethers and 2-aminothiophenol with $CpRu^{II}Cl(PPh_3)_2$ (Cp^- = cyclopentadienyl anion), under identical reaction conditions, are reported. While 2-(methylthio)aniline, H_2L^1 and an analogous substrate, 2-(phenylthio)-aniline yielded dicationic dinuclear complexes $[(PPh_3)CpRu^{II}(L^3/L^4)-Ru^{II}Cp(PPh_3)]Cl_2$ (where L^3 = (4*E*)-4-(4-imino-3-(methylthio)-cyclohexa-2,5-dienylidene)-2-(methylthio)cyclohexa-2,5-dienimine ($[\mathbf{1a}]Cl_2$) and L^4 = (4*E*)-4-(4-imino-3-(phenylthio)cyclohexa-2,5-dienylidene)-2-(phenylthio)cyclohexa-2,5-dienimine ($[\mathbf{1b}]Cl_2$)), the reaction with 2-aminothiophenol (H_2L^2) produced a mononuclear complex $[(PPh_3)CpRu^{II}(L^2)]Cl$ (where L^2 = 6-iminocyclohexa-2,4-dienethione) ($[\mathbf{2}]Cl$). All these complexes are obtained in high yields (65%−75%). Formations of the products from the above reactions involve a similar level of oxidation of the respective substrate, although their courses are completely different. A comparison between the above two chemical transformations are scrutinized thoroughly. Characterizations of these complexes were made using a host of physical methods: X-ray crystallography, nuclear magnetic resonance (NMR), cyclic voltammetry, ultraviolet−visible (UV-vis), electron paramagnetic resonance (EPR) spectroscopy, and density functional theory (DFT). The complexes $[\mathbf{1a}]Cl_2$ and $[\mathbf{1b}]Cl_2$ showed intense metal-to-ligand charge transfer transition in the long wavelength region of the spectrum, at 860 and 895 nm, respectively, and displayed two reversible electron transfer (ET) processes at $[\mathbf{1a}]^{2+}$: −0.28 and −0.52 V; $[\mathbf{1b}]^{2+}$: −0.13 and −0.47 V, along with an irreversible ET process at 0.76 and 0.54 V, respectively. The ET processes at negative potentials are due to successive reductions of the bridging ligand, which are characterized by EPR and UV-vis spectroscopy. The one-electron reduced compound, $[\mathbf{1a}]^+$, showed a intraligand charge transfer transition (ILCT) at 1530 nm. The complex $[\mathbf{2}]^+$ showed a reversible ET process at −0.36 V and two irreversible ET processes at −1.04 and 1.18 V, respectively. DFT calculations were used to support the spectral and redox properties of the complexes and also to throw light on the difference of redox behavior between thioether and thiophenol substrates.

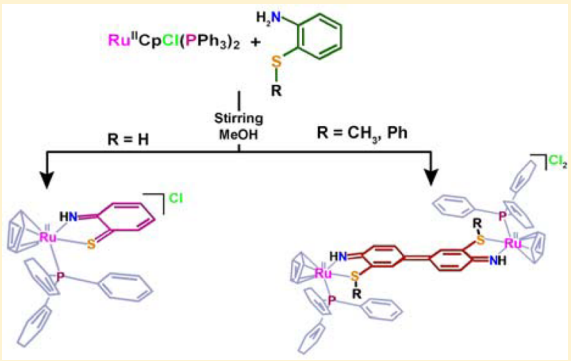

INTRODUCTION

Studies on redox-mediated chemical reaction in transition metal complexes of redox noninnocent ligands is an emerging field of current research.[1] Synergistic participation of metal and ligand redox has developed an attractive avenue for small molecule transformations[2] (both catalytic and stoichiometric). For example, metalloenzymes often selects redox active ligand(s) and metal to bring about controlled multielectron processes during many biochemical transformations.[3] Basic research in this area has been primarily confined to redox-active chelating ligands: symmetrical ligands (such as catechol,[4] diamine,[5] dithiol,[6] etc.) and unsymmetrical ones (such as aminophenol,[7] aminothiophenol,[8] etc.). In these ligands, the three variable valence states (Scheme 1) of the coordinated ligand(s) involve a fully reduced catecholate dianion and a fully oxidized neutral quinone, along with a partially oxidized semiquinone monoradical intermediate.[9]

Scheme 1

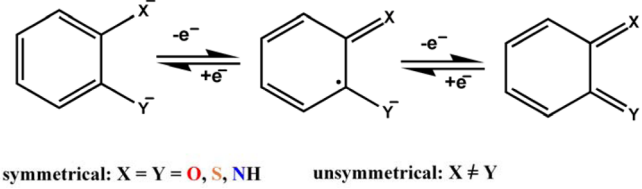

In comparison, the corresponding redox chemistry of ligands bearing only one oxidizable redox active donor site[10] as that in

Received: February 26, 2015
Published: June 24, 2015

DOI: 10.1021/acs.inorgchem.5b00457
Inorg. Chem. 2015, 54, 6235−6244

2-aminothioether[11] is different, since it can undergo usual one-electron ligand oxidation, producing a reactive radical intermediate. Thus, unusual chemical behavior of the oxidized aminothioether complexes of above substrate when coordinated especially to a diamagnetic metal center is anticipated.

The present work stems from our previous observations[11,12] on the chemical reactions of coordinated 2-(methylthio)anilide producing unexpected products via *ortho* C−H and *para* C−H activation of the phenyl ring. It was argued[11] that partial oxidation of coordinated 2-(methylthio)anilide and subsequent nucleophilic addition (vis-à-vis, oxidation of the intermediate(s)) led to the above products. Given this background, we now purposefully plan a stoichiometric reaction between 2-(methythio)aniline (H_2L^1) and the complex, $CpRu^{II}Cl(PPh_3)_2$ with an anticipation of *para* C−H activation. The reaction resulted a unique bimetallic Ru_2^{II}-complex of a new tetradentate bridging ligand containing a rigid NH-$(CH_3S)C_6H_3$−$C_6H_3(SCH_3)$−NH moiety via C−C coupling reaction. To have an insight into the above chemical reaction a similar chemical reaction with 2-aminothiophenol (H_2L^2) with the above ruthenium complex is investigated, which yielded a monometallic complex, as expected. The isolated complexes were characterized thoroughly by redox, spectroscopic methods and analysis of molecular and electronic structures. A comparison of the above two reactions has not only revealed knowledge on the redox behavior of coordinated 2-(methylthio)anilide, but also has cast light on the redox-initiated reactivity pattern of the redox active ligands that contain a single oxidizable redox active center.

RESULTS AND DISCUSSION

The chemical reaction of 2-(methylthio)aniline (H_2L^1) with $CpRu^{II}Cl(PPh_3)_2$ (in 1:1 molar proportion) at 300 K proceeded cleanly in methanol. The initial yellow color of the solution gradually turned dull green within 6 h. The crude product, obtained after evaporation of solvent, was purified using a preparative TLC technique. TLC experiment showed the presence of a major green band, which, after separation and follow-up treatment (see the Experimental Section) yielded a dicationic binuclear green complex of composition $[(PPh_3)CpRu^{II}L^3Ru^{II}Cp(PPh_3)]Cl_2$ ($[\mathbf{1a}]Cl_2$) in a high yield (avg 70%). In this reaction, a bis-chelated NH-$(CH_3S)C_6H_3$−$C_6H_3(SCH_3)$-NH bridging ligand L^3 (where L^3 = (4*E*)-4-(4-imino-3-(methylthio)cyclohexa-2,5-dienylidene)-2-(methylthio)cyclohexa-2,5-dienimine) was generated *in situ* via an unusual C−C bond formation reaction that acts as a bridge for connecting two $[CpRu^{II}(PPh_3)]$ moieties via bis-chelation, as shown in Scheme 2. A similar reaction of $CpRu^{II}Cl(PPh_3)_2$ with 2-(phenylthio)aniline produced a compound, $[(PPh_3)CpRu^{II}L^4Ru^{II}Cp(PPh_3)]Cl_2$ (where L^4 = (4E)-4-(4-imino-3-(phenylthio)cyclohexa-2,5-dienylidene)-2-(phenylthio)-cyclohexa-2,5-dienimine) (referenced hereafter as $[\mathbf{1b}]Cl_2$), establishing that the reaction is a general one. The overall chemical reaction is shown in Scheme 2.

To follow the above reaction further, a parallel reaction with the corresponding thiol, 2-aminothiophenol (H_2L^2), was performed. In this reactant, the thiol proton is dissociable and the redox behavior of coordinated thiolato function is different than that of the thio-ether substrate. Under identical conditions, the reaction resulted a monometallic complex [**2**]Cl of the ligand, 6-iminocyclohexa-2,4-dienethione, L^2 in almost quantitative yield. The chemical reaction is shown in Scheme 3.

Scheme 2. Synthesis of Complexes $[\mathbf{1a}]Cl_2$ and $[\mathbf{1b}]Cl_2$: (a) Overall Reaction and (b) Schematic Presentation

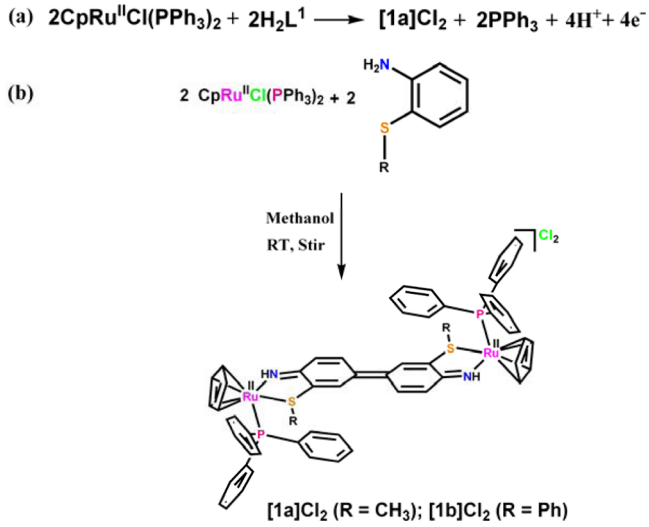

Scheme 3. Synthesis of Complex [2]Cl: (a) Overall Reaction and (b) Schematic Presentation

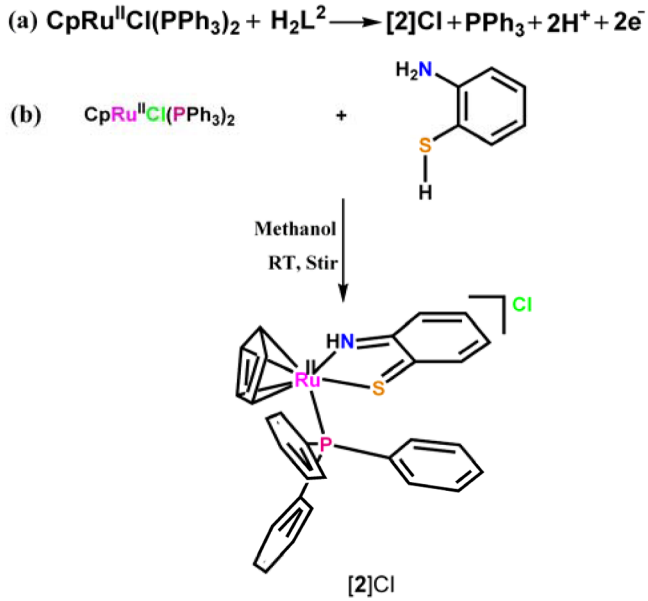

Formulation and Characterization. Electrospray ionization mass spectra of the complexes $[\mathbf{1a}]Cl_2$ and $[\mathbf{1b}]Cl_2$ corroborate with their formulations as $[(PPh_3)CpRu^{II}(L^3/L^4)Ru^{II}Cp(PPh_3)]Cl_2$: these showed an intense peak, at *m*/*z* 566 and 628 amu, respectively, that was due to $([M]^{2+}/2)$, where "M" represents the molecular mass of $[\mathbf{1a}]^{2+}/[\mathbf{1b}]^{2+}$. The spectrum of the complex [**2**]Cl displayed a peak at *m*/*z* 552 amu, because of the molecular ion $[(PPh_3)CpRu^{II}(L^2)]^+$. Moreover, the experimental spectral features of the spectra match well with their simulated isotopic patterns for the given formulations. ESI-MS spectra of the compound together with the simulated spectra are submitted in the Figures S1−S3 in the Supporting Information. Their compositions were verified further by their elemental analyses (cf., see the Experimental Section).

The complexes $[\mathbf{1a}]Cl_2$, $[\mathbf{1b}]Cl_2$, and [**2**]Cl all possess an *S* = 0 ground state, as determined by their magnetic susceptibility

DOI: 10.1021/acs.inorgchem.5b00457
Inorg. Chem. 2015, 54, 6235−6244

measurements at room temperature. These displayed sharp ^{1}H NMR signals in the normal range for diamagnetic compounds. The low number of resonances for the complexes [**1a**]Cl_2 and [**1b**]Cl_2 indicate high symmetry of the molecules in solutions. Signal due to imino (═NH) proton resonance of the bridging ligands L^3 and L^4 appeared at δ 8.6 and 6.9 ppm, respectively, which disappeared on D_2O shake. The aromatic proton resonances of the complex [**1a**]Cl_2 appeared in the region 7.7−6.8 ppm. Proton resonances from the L^3 ligand appeared as a doublet at 7.75, a singlet at 6.80 ppm and another one proton signal overlapped with the −PPh_3 protons. The methyl and cyclopentadienyl ring proton resonances of [**1a**]Cl_2 appeared at δ, 2.7 and 4.9 ppm, respectively. Because of serious overlap of proton resonances for [**1b**]Cl_2 (S-Ph, −PPh_3, and L^4) the assignment of aromatic protons signals was not possible. However, cyclopentadienyl ring protons of [**1b**]Cl_2 appeared at 4.57 (3H) and 4.62 (2H) ppm. The ^{1}H NMR spectrum of the compound [**2**]Cl appeared in the region of 7.4−6.8 ppm: two triplet proton resonances appeared at 6.8 and 7.0 ppm, one doublet signal appeared at 7.47 ppm, and another resonance overlapped with the phenyl proton resonances. A signal due to imino (═NH) proton resonance of the ligand L^2 appeared at δ 15.3, which disappeared on D_2O shake. The ^{1}H NMR spectra of [**1a**]Cl_2, [**1b**]Cl_2, and [**2**]Cl are submitted as Supporting Information (Figures S4−S6).

X-ray Crystal Structures. X-ray diffraction (XRD)-quality single crystals of the complex [**1a**]Cl_2 were obtained by slow evaporation of its solution in dichloromethane-methanol (1:1) solvent mixture. ORTEP presentation of the cationic complex [**1a**]$^{2+}$ with partial atom numbering scheme is displayed in Figure 1, and metrical parameters are collected in Table 1.

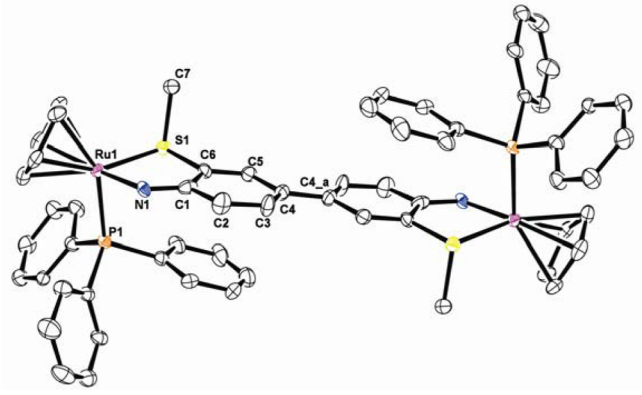

Figure 1. ORTEP and partial atom numbering scheme of [**1a**]$^{2+}$. Counter anions (Cl^-), water (H_2O) molecules, and all hydrogen atoms are omitted for clarity.

X-ray crystal structure analysis of [**1a**]Cl_2 confirmed its formulation as a Ru_2-complex. The asymmetric unit of the complex consists of a cationic molecule [**1a**]$^{2+}$ and two Cl^- as counteranions. Each ruthenium center is coordinated to one bidentate end (N,S) of the bridging ligand (L^3), one monoanionic cyclopentadienyl ring, and one neutral PPh_3 ligand (see Figure 1). The molecule resides on a crystallographic center of symmetry, where the two [$(PPh_3)CpRu^{II}L^1$] fragments are equivalent. The two C_6H_3 units of the bridging ligand are planar[13] and the two PPh_3 and methyl groups are oriented *anti* to this plane. The Ru−N1 bond distance is 2.049(6) Å, which is comparable to the observed Ru^{II}−N(imine) bond distances in previously known[12,14] imine

Table 1. Selected Bond Distances and Bond Angles of Complexes [1a]$^{2+}$, [1a]$^+$, and [1a]^0

	[1a]$^{2+}$		[1a]$^+$	[1a]^0
parameter	expt	calcd	calcd	calcd
Bond Lengths (Å)				
Ru1−S1	2.359(2)	2.452	2.437	2.4311
Ru1−P1	2.320(2)	2.408	2.385	2.355
Ru1−N1	2.049(6)	2.045	2.085	2.103
S1−C6	1.776(6)	1.803	1.799	1.7956
N1−C1	1.298(8)	1.327	1.337	1.349
C1−C6	1.432(9)	1.439	1.431	1.423
C1−C2	1.443(10)	1.435	1.431	1.427
C2−C3	1.380(10)	1.366	1.374	1.383
C3−C4	1.443(10)	1.439	1.426	1.416
C4−C5	1.414(8)	1.437	1.420	1.403
C4−C4_a	1.438(9)	1.432	1.452	1.479
C5−C6	1.375(9)	1.367	1.379	1.395
Bond Angles (deg)				
S1−Ru1−P1	88.22(6)	90.605	91.618	93.012
S1−Ru1−N1	81.91(13)	79.777	79.850	79.85
P1−Ru1−N1	91.46(14)	93.307	90.675	88.352
Ru1−N1−C1	122.2(4)	126.603	124.903	123.344
Ru1−S1−C6	98.9(2)	98.980	99.697	100.10

complexes. The bond distance, (C4−C4_a) between the two fused rings is 1.438(9) Å, which is shorter[15,16] than a typical C−C single bond (1.54 Å). For example, a similar C−C bond length (1.425(10) Å) was reported[15] in a closely related Ru_2-complex, [$TpRu\{P(OMe)_3\}_2NH(C_6H_4$-)$]_2[OTf]_2$ (where Tp = hydridotris(pyrazolylborate). In addition, the N1−C1 bond distance (1.298(8) Å) is shorter than expected for a N−C single bond length (1.47 Å).[11,12] Similar trend of bond lengths were noted previously in several related imino complexes.[8] The S1−C6 bond distance (1.776(6) Å) is similar to that of typical S−C single bond length.[17] Notably, the C2−C3 and C5−C6 bond lengths 1.380(10) and 1.375(9) Å, respectively are significantly shorter than the bond lengths of C1−C2 (1.443(10) Å), C4−C5 (1.414(8) Å), C1−C6 (1.432(9) Å), and C3−C4 (1.443(10) Å), indicating quinoid-type localization of the π-electrons in the C_6H_3 rings. It is worth noting here that L^3 is redox noninnocent and this issue has been addressed in a later section. Since the ligand L^3, in this complex, coordinates as a neutral (oxidized) ligand, the oxidation state of the two ruthenium centers in the complex is +2. Assessment of oxidation states has also been supported by the analyses of EPR spectrum of the electrogenerated species and scrutiny of the results of DFT calculations. Binuclear ruthenium complexes of biphenyl bridging ligands bearing O,O and O,N, as well as N,N donors, have been known in the literature;[9c,18] however, complexes that contain the oxidized quinone form with planar orientation of the two rings is rarely observed.[15]

The chloride salt of the cationic complex [**2**]$^+$ is microcrystalline; however, its hexafluorophosphate salt [**2**]PF_6 formed suitable crystals for single-crystal X-ray structure determination. Its ORTEP presentation and partial atom numbering scheme are shown in Figure 2, and selected bond parameters are collected in Table 2. The X-ray structure of this complex revealed that the ruthenium center is coordinated to a neutral bidentate ligand L^2, one monoanionic cyclopentadienyl ring, and one neutral PPh_3 ligand. The Ru−N1 bond distance is 1.970(3) Å, which is comparable to that in previously reported Ru^{II}-imine complexes.[14] The most notable feature in this

DOI: 10.1021/acs.inorgchem.5b00457
Inorg. Chem. 2015, 54, 6235−6244

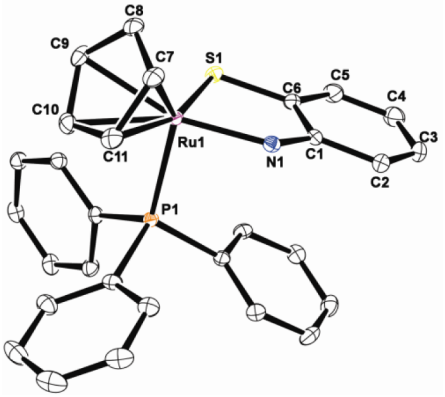

Figure 2. ORTEP and partial atom numbering scheme of $[2]^+$. Counter anion (PF_6^-) and hydrogen atoms are omitted for clarity.

Table 2. Selected Bond Distances in Complexes $[2]^+$ and $[2]^0$

	Bond Length (Å)		
	Expt	Calcd	
parameter	$[2]^+$	$[2]^+$	$[2]^0$
Ru1−N1	1.970(3)	1.988	2.044
Ru1−S1	2.2620(16)	2.320	2.383
Ru1−P1	2.3332(16)	2.398	2.337
N1−C1	1.329(5)	1.340	1.358
S1−C6	1.691(4)	1.710	1.743
C1−C2	1.422(5)	1.428	1.424
C2−C3	1.351(6)	1.370	1.380
C3−C4	1.406(6)	1.426	1.412
C4−C5	1.362(6)	1.376	1.387
C5−C6	1.409(6)	1.416	1.407
C6−C1	1.425(6)	1.440	1.431

structure is the short C−S bond distance and, in fact, is a typical double bond.[19] Moreover, this bond is considerably shorter than that in the Ru_2-complex, $[1a]^{2+}$: 1.691(4) $[2]^+$ (C6−S1) versus 1.776(6) Å $[1a]^{2+}$ (C6−S1). Furthermore, the N1−C1 bond distance (1.329(5) Å) is much shorter than a N−C single bond implying a double bond[11,12] character. The bond pairs C1−C2 and C5−C6 (1.422(5) and 1.409(6) Å, respectively) are single bonds, while the bond pairs C2−C3 and C4−C5 are double bonds with bond lengths of 1.351(6) and 1.362(6) Å, respectively. This trend is a clear indication of a quinoid oxidation state of L^2. Thus, the metrical parameters indicated that the ruthenium ion in this complex is bivalent and the charge is satisfied by one cyclopentadienyl anion and one counterion: hexafluorophosphate.

Cyclic Voltammetry and EPR. Redox properties of all the complexes $[1a]^{2+}$, $[1b]^{2+}$, and $[2]^+$ were examined by cyclic voltammetry in acetonitrile solution containing 0.1 M $[Et_4N]ClO_4$ as the supporting electrolyte in the potential range from +1.8 V to −1.5 V, using platinum disk as the working electrode. The potentials are referenced to the saturated Ag/AgCl electrode, and the results are summarized in Table 3. The $E_{1/2}$ value of the ferrocenium−ferrocene couple under our experimental conditions was 0.40 V. The stoichiometry of the redox processes was confirmed by the coulomb count of constant-potential electrolysis experiments for the reversible waves.

Table 3. Cyclic Voltammetric Data and UV-vis-NIR Spectral Data of $[1a]^{2+}$, $[1b]^{2+}$, and $[2]^+$

	Cyclic Voltammetric Data[a]		UV-vis Spectral Data[b]	
compound	$E_{1/2}$[c] (V)	ΔE_p (mV)	λ_{max} (nm)	ε[b] (M^{-1} cm^{-1})
$[1a]^{2+}$	0.76[d]		940[e]	5.8×10^4
	−0.28	90	860	
	−0.52	90	460	1.03×10^4
			315	1.8×10^4
$[1b]^{2+}$	0.54[d]		895	4.1×10^4
	−0.13	90	477	0.8×10^4
	−0.47	90	310	1.3×10^4
$[2]^+$	1.18[d]		800[e]	
	−0.36		470	1.57×10^4
	−1.04[d]	70		

[a]Acetonitrile solution (supporting electrolyte $[Et_4N]ClO_4$), reference electrode Ag/AgCl. [b]Molar extinction coefficients in acetonitrile solvent. [c]$E_{1/2} = 0.5(E_{pa} + E_{pc})$, where E_{pa} and E_{pc} are anodic and cathodic peak potentials, respectively. $\Delta E_p = E_{pa} - E_{pc}$, scan rate = 50 mV s^{-1}. [d]Irreversible. [e]Shoulder.

Cyclic voltammetry of complex $[1a]^{2+}$ exhibits two reversible electron transfer (ET) processes at potentials −0.28 and −0.52 V, together with one irreversible ET process at a potential of 0.76 V (Figure 3). Similarly, complex $[1b]^{2+}$ showed two

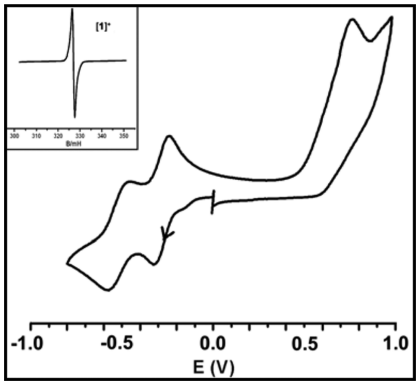

Figure 3. Cyclic voltammogram of complex $[1a]^{2+}$. The EPR spectrum of the electrogenerated complex $[1a]^+$ is shown in the inset.

reversible ET processes, at potentials of −0.13 and −0.47 V, and an irreversible ET process at a potential of 0.54 V (see Figure S7 in the Supporting Information). Complex $[2]^+$, on the other hand, showed one reversible ET process at a potential of −0.36 V and two irreversible ET processes at −1.04 V and 1.18 V (see Figure 4). To gain further insight into the electron transfer events associated with the reversible ET processes, the EPR spectra of the electrogenerated reduced complexes were studied at 120 K. The monocationic complex $[1a]^+$, generated by exhaustive electrolysis at −0.30 V, showed a ligand centered single line EPR spectrum (Figure 3, inset) at g = 1.999. However, attempts to study the neutral complex [1a] by bulk electrolysis (at −0.70 V) failed because of the unstable nature of the generated compound. Similar EPR spectral results were also observed for compound $[1b]^{2+}$. DFT analyses of the complexes, $[1a]^{2+}$, $[1a]^+$, and $[1a]^0$ have revealed successive reductions of the bridging ligands (see later discussion), as shown in Scheme 4.

DOI: 10.1021/acs.inorgchem.5b00457
Inorg. Chem. 2015, 54, 6235−6244

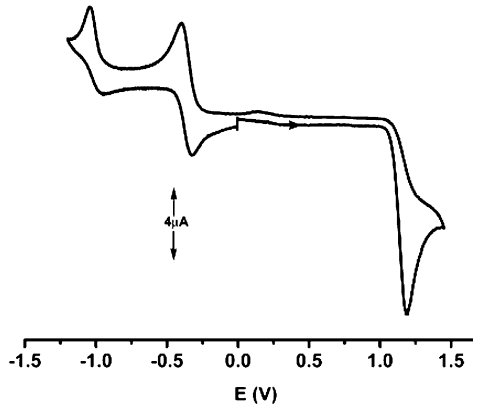

Figure 4. Cyclic voltammogram of complex $[\mathbf{2}]^{+}$ in an acetonitrile solvent.

However, the metal-centered oxidation (Ru^{II}/Ru^{III}) of the above complex is irreversible and is attributed to degradation of the complex upon electron transfer. The monometallic brown compound $[\mathbf{2}]^{+}$, upon electrolysis at −0.56 V, became intense blue and the one-electron-reduced compound is EPR active, which showed an almost isotropic signal at $g = 1.992$ with little metal contributions (see Figure S8 in the Supporting Information). Accordingly, this response is assigned to the reduction of the coordinated *ortho*-thioquinoneimine ligand.

Electronic Structures of $[\mathbf{1a}]^{+2/+1/0}$ and $[\mathbf{2}]^{+/0}$. Because of the redox noninnocence nature of both the bridging ligand and the ruthenium metal, the assignment of electronic structures of the redox isomers of $[\mathbf{1a}]^{z+}$ ($z = +2, +1, 0$) is an important issue in the context of their multiple electronic structure possibilities. Notably, the *in situ* formed bridging ligand, L^3, can formally exist in three redox states: neutral, L^3; radical monoanion $[L^3]^{\bullet -}$; and dianion $[L^3]^{2-}$. The following two possible electronic structure descriptions of the diamagnetic complex $[\mathbf{1a}]^{2+}$ were considered: (i) $[(PPh_3)CpRu^{II}(L^3)^0Ru^{II}Cp(PPh_3)]^{2+}$ and (ii) $[(PPh_3)CpRu^{III}(L^3)^{2-}Ru^{III}Cp(PPh_3)]^{2+}$, where $(L^3)^0$ and $(L^3)^{2-}$ are as shown in Scheme 4. Diamagnetism of description (ii) is due to complete spin-pairing via antiferromagnetic coupling between the unpaired spins on two Ru^{III} (d^5) atoms and the unpaired spins of the radical bridging ligand. This description is energetically higher than the former by 0.97 eV/mol (see Table S1 in the Supporting Information). Moreover, the calculated metrical parameters for the former description are closer to the crystallographically observed metrical parameters, which are collected in Table S1 in the Supporting Information.

The energies and compositions of the DFT calculated frontier orbitals of $[\mathbf{1a}]^{2+}$ are summarized in the Supporting Information (Table S2). Analyses of the molecular orbitals of the complexes reveal that the highest occupied MO (HOMO) is formed by a combination of metal *d* orbitals and the bridging ligand orbitals, with the major contribution coming from the metal orbitals (Ru, 47% and L^3, 27%). Closely lying occupied orbitals HOMO-1 and HOMO-2 are formed by a combination of metal *d* orbitals (major) and L^3 ligand orbitals (HOMO-1: Ru, 57%, L^3, 9%; and HOMO-2: Ru, 58%, L^3, 10%). The lowest unoccupied molecular orbital (LUMO) is represented primarily by ligand orbitals with minor contributions of the metal center (Ru, 19% and L^3, 58%), whereas the LUMO+1 orbital is fully localized over the ligand orbitals (92%). The electron density distributions of HOMOs and LUMOs, with their relative contributions from metal and ligand orbitals, are shown in the Supporting Information (Table S2 and Figure S9).

Geometry optimizations were also carried out on its two redox isomers: $[\mathbf{1a}]^{+}$ and $[\mathbf{1a}]^{0}$. Optimized structural parameters for the computed ground states of these are collected in Table 1; molecular orbitals for the computed ground states of $[\mathbf{1a}]^{+}$ and $[\mathbf{1a}]^{0}$ are listed in Tables S3 and S4 in the Supporting Information, respectively, and are depicted in Figures S10 and S11 in the Supporting Information, respectively. The partially reduced complex $[\mathbf{1a}]^{+}$ has a doublet ground state (Figure 3, inset), and the net spin density plot (see the Supporting Information (Figure S12)) indicates that the first reduction occurs at the ligand center. The two-electron-reduced neutral complex $[\mathbf{1a}]^{0}$ has a closed-shell singlet state, which again is a ligand-centered redox process. Overall oxidation states of metal and ligand in the isolated dicationic complex and two successive reduced complexes may therefore be described as $[(PPh_3)CpRu^{II}(L^3)Ru^{II}Cp(PPh_3)]^{2+}$, $[(PPh_3)CpRu^{II}(L_3)^{\bullet -}Ru^{II}Cp(PPh_3)]^{+}$ and $[(PPh_3)CpRu^{II}(L^3)^{2-}Ru^{II}Cp(PPh_3)]^{0}$, respectively. Significantly, the two connected rings in the dication are planar while that in the monocation and in the neutral complex[20] both are nonplanar with dihedral angles[13] of 19.96° $[\mathbf{1a}]^{+}$ and 33.45° $[\mathbf{1a}]^{0}$, respectively. Moreover, there is a gradual elongation of the connecting C−C bond length in the same order: 1.432 Å < 1.452 Å < 1.479 Å. All of these factors taken together, we conclude that the successive step electron transfer in $[\mathbf{1a}]^{2+}$ occur at the bridging ligand, as shown in Scheme 4.

The monometallic complex $[\mathbf{2}]^{+}$ is optimized in a closed-shell singlet and the optimized metrical parameters matched well with the experimentally observed parameters (see Table 2). The HOMO is localized over the L^2 ligand (50%) and Ru atom (40%), whereas LUMO is primarily localized on the L^2 ligand (65%) (see Figure S13 and Table S5 in the Supporting Information). The one-electron-reduced complex $[\mathbf{2}]^{0}$ has a doublet ground state with the spin localization (Figure S14 in the Supporting Information) mainly over the L^2 ligand (∼75%) and a small part of it resides on the Ru-metal orbitals (∼20%),

Scheme 4. Observed Two-Step Reductions of Ligand L^3

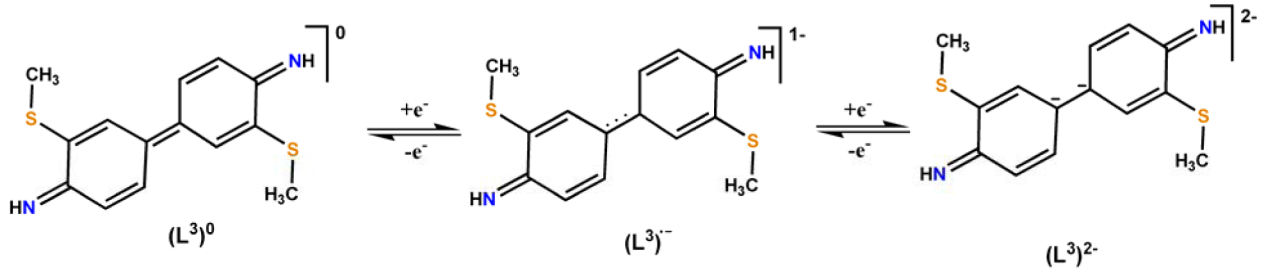

DOI: 10.1021/acs.inorgchem.5b00457
Inorg. Chem. 2015, 54, 6235−6244

which is consistent with the observed small anisotropy in the EPR spectrum of $[\mathbf{2}]^0$ (Figure S8 in the Supporting Information).

Electronic Spectra. Electronic spectra of the compounds $[\mathbf{1a}]^{2+}$, $[\mathbf{1b}]^{2+}$, and $[\mathbf{2}]^{+}$ were recorded in acetonitrile solution. The experimental spectral results are collected in Table 3, and two representative spectra of $[\mathbf{1a}]^{2+}$ and $[\mathbf{2}]^{+}$ are displayed in Figures 5-6, respectively. Assignments of spectral transitions are guided by the results of TD-DFT calculations on the complexes. The calculated excitation energies using TD-DFT for the complex are collected in Tables S6 and S7 in the Supporting Information. The color of the solutions changes upon reduction. For example, the color of the respective complexes are green $[\mathbf{1a}]^{2+}$, dull green $[\mathbf{1a}]^{+}$, brown $[\mathbf{2}]^{+}$, and blue $[\mathbf{2}]^{0}$. Spectral changes are shown in Figures 5 and 6, respectively.

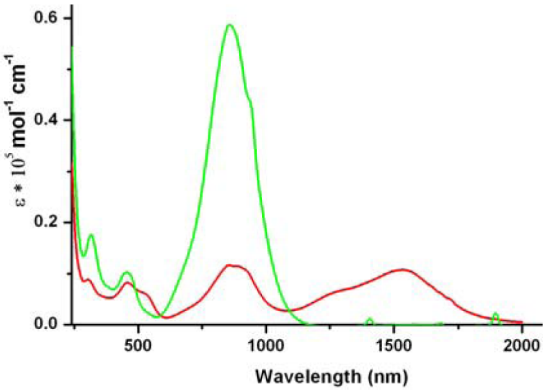

Figure 5. UV-vis-NIR spectra of complexes $[\mathbf{1a}]^{2+}$ (green) and $[\mathbf{1a}]^{+}$ (red).

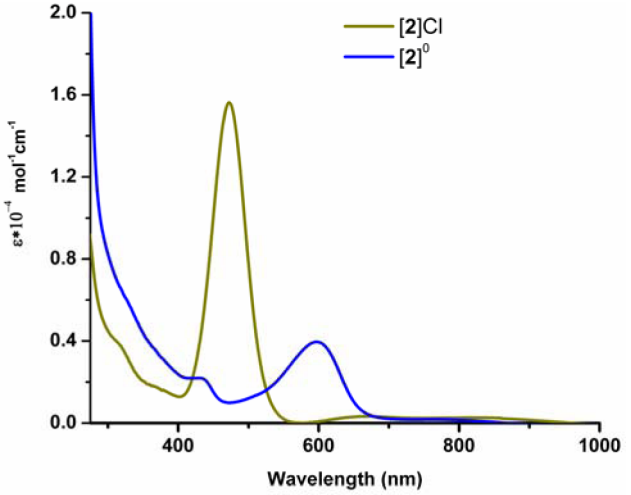

Figure 6. UV-vis-NIR spectra of complexes $[\mathbf{2}]^{+}$ and $[\mathbf{2}]^{0}$.

The complexes, $[\mathbf{1a}]^{2+}$ and $[\mathbf{1b}]^{2+}$ exhibited an intense low-energy transition in the NIR region at 860 and 895 nm, respectively. This transition of $[\mathbf{1a}]^{2+}$ compared well with the HOMO/HOMO-2 → LUMO transition: for comparison, the TD-DFT value appeared at 890 nm (Table S6 in the Supporting Information). Thus, the transition may be ascribed as a metal-to-ligand charge transfer transition (MLCT, see before). Upon one-electron reduction, this MLCT band in $[\mathbf{1a}]^{+}$ shifted slightly to lower energy at 880 nm but its intensity diminished considerably, together with the appearance of a weak and broad band near 1535 nm (ε = 1.06 × 10^4 M^{-1} cm^{-1}). The electronic transition of $[\mathbf{1a}]^{+}$ compared well with a HOMO(β) → LUMO(β) transition: the TD-DFT value appeared at 1387 nm (Table S6 in the Supporting Information). Notably, HOMO(β) is delocalized over the metal (38%) and ligand (41%) orbitals, whereas the LUMO(β) is primarily delocalized over the ligand (65%) orbitals (see Table S3 in the Supporting Information). Thus, this transition may be attributed primarily to intraligand charge-transfer (ILCT) transition. This low-energy ILCT transition in $[\mathbf{1a}]^{+}$, as expected, is due to partial reduction of the bridging ligand.

Complex $[\mathbf{2}]^{+}$ is brown in color and absorbs strongly at 470 nm. Based on the values of the oscillator strength predicted by using TD-DFT, the most intense transition at 470 nm for compound $[\mathbf{2}]^{+}$ is ascribed to the excitation from the HOMO-1 → LUMO (46%) transition and the HOMO-2 → LUMO (44%) transition; the corresponding transition (calculated) appeared at 480 nm (Table S7 in the Supporting Information). The one-electron-reduced compound, $[\mathbf{2}]^{0}$, is blue in color and absorbs strongly at 600 nm. The experimental transitions compared well with the calculated (580 nm) values for the HOMO-2(β) → LUMO(β) (82%) transition. Note that the orbital HOMO-2(β) is delocalized over Ru (52%) and L^2 (37%) orbitals, whereas the LUMO(β) is primarily delocalized over the L^2 (72%) ligand (see Figure S15 and Table S8 in the Supporting Information). Thus, this transition may be attributed to charge transfer from a mixed metal−ligand orbital to a ligand orbital.

Scheme 5. Overall Redox Events Occurring at H_2L^1 and H_2L^2

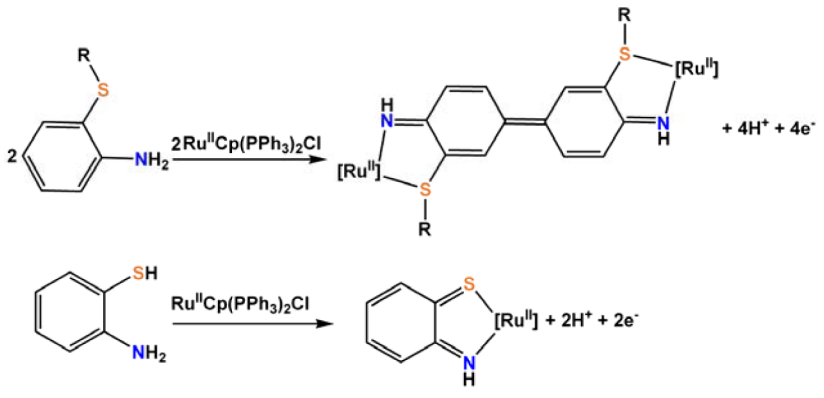

DOI: 10.1021/acs.inorgchem.5b00457
Inorg. Chem. 2015, 54, 6235−6244

Rational of Chemical Transformations. Based on the above results, we note that, in the above two reference chemical reactions, there is no change of redox state of metal ion (Ru^{II}), but the 2-substituted aniline substrates underwent oxidation [$-(2e^- + 2H^+)$/mol] during the reactions. The chemical transformations of the above two substrates are as shown in Scheme 5.

We also note here that the oxidation of deprotonated 2-aminothiophenol is usual and follows the literature report[8,9] on it and its closely related substrates. However, similar $2e^-$ oxidation of anilidothio-ether is not possible, because of the redox innocent character of the C-SR bond, although delocalization of unpaired spin of one electron in the partially oxidized monocation of coordinated deprontonated amine (as shown in Scheme 6) is a genuine possibility. Subsequent

Scheme 6. Proposed Redox Tautomers of Partially Oxidized HL^1 and Step Subsequent Chemical Transformation

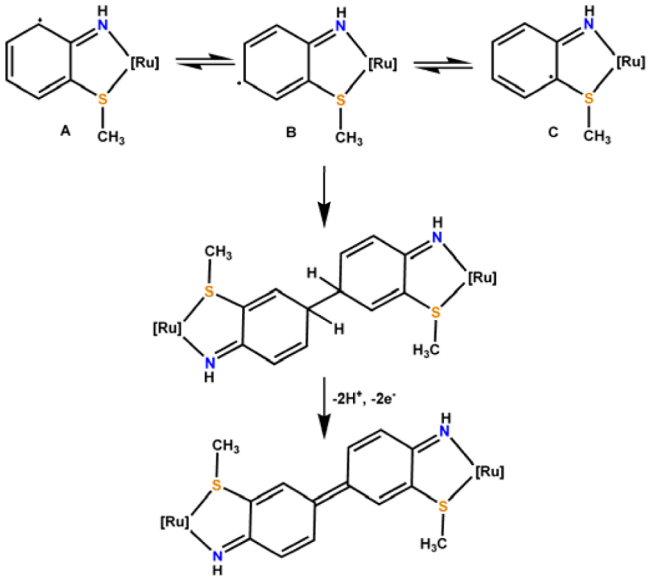

oxidative dimerization of the above intermediate radical has resulted the bis-chelated tetradentate ligand. To establish our above proposition, a series of following reactions were investigated. First, the above reaction of anilidothio ether does not proceed at all under deaerated conditions or in the presence of a radical scavenger, TEMPO (where TEMPO = 2,2′,6,6′-tetramethylpiperidinoxyl). Second, the above reaction of 2-thioether substituted aniline, in air, produced a dull-green intermediate within about an hour, which, upon further stirring, produces the final intense green product within 6 h.

The intermediate complex (dull green product), however, was not isolable but its spectral properties were studied: (i) ESI-MS spectrum matches well with a composition, $[RuCp(HL^1)PPh_3]^+$ (Figure S16 in the Supporting Information) and (ii) the EPR spectrum of the solution showed a ligand-centered radical-like isotropic spectrum at $g = 1.997$ (Figure S17 in the Supporting Information). Therefore, it is likely that a ligand radical compound intermediate originated,[15,21] because of partial oxidation of the deprotonated amine. A blank experiment that consisted of 1 h of stirring of a methanolic solution of H_2L^1 did not produce the paramagnetic solution, which excluded the possibility of oxidation of free amine in the above reaction. Furthermore, the results of DFT calculations also revealed the presence of unpaired spin in the partially oxidized complex, $[CpRu^{II}(HL^1)PPh_3]^+$, which is primarily delocalized over the phenyl ring (Figure S18 in the Supporting Information) making it susceptible toward an oxidative homo coupling[15] reaction to result in the final product. Here, we also compare the charge distributions in DFT generated between the complex intermediates, $[CpRu^{II}(HL^1)PPh_3]^+$ and $[CpRu^{II}(L^2)PPh_3]$, $[\mathbf{2}]^0$. In the later complex, a significant part of the unpaired spin is distributed over S (∼22%) and N (∼32%) (see Figure S14 in the Supporting Information), whereas that in the former is located on N (∼38%), and the phenyl ring (∼40%), and virtually no spin over the S atom.

CONCLUSION

The present work has further demonstrated that 2-aminothioether is an excellent candidate for the study of redox-induced C−C coupling reactions at the phenyl ring that otherwise do not occur. Upon one-electron oxidation, the coordinated 2-thioether-substituted anilido substrate produces a radical that is delocalized over the aryl ring, thus developing the possibility of radical-induced chemical reactions at the aromatic ring. Previously, we noted[11] an example of aromatic ring hydroxylation of coordinated 2-(methylthio)anilide substrate. In the present case, an example of dimerization via C−C coupling between the two activated phenyl rings is noted. The resulting Ru_2-complex containing a planar bridging ligand is noteworthy, because this belongs to a rare category[15] of compounds that are of interest[22] for various reasons. Furthermore, redox properties in this system have been successfully followed, using various spectroscopic techniques and DFT analysis.

EXPERIMENTAL SECTION

Materials. The starting compound, $RuCl_3$ was collected from Arora−Matthey (Kolkata, India). The ligands 2-(methylthio)aniline, 2-aminothiophenol, and 2-(phenylthio)aniline were purchased from Sigma−Aldrich, Fluka, and Acros Chemicals, respectively. The mediator complex $CpRu^{II}Cl(PPh_3)_2$[23] and the supporting electrolyte tetraethylammonium perchlorate, $[Et_4N]ClO_4$,[24] were prepared and crystallized following published procedures. *[**Caution!** Perchlorate salts must be handled with care and appropriate safety precautions.]* Solvents and chemicals used for syntheses were of analytical grade and used as received.

Instrumentation. UV-vis-NIR absorption spectra were recorded either on a Perkin−Elmer Model Lambda 950 UV/vis spectrophotometer or on a J&M TIDAS instrument. The infrared (IR) spectra were recorded with a Perkin−Elmer Model 783 spectrophotometer. Cyclic voltammetry was carried out in 0.1 M $[Et_4N]ClO_4$ solutions, using a three-electrode configuration (platinum working electrode, platinum counter electrode, Ag/AgCl reference electrode) and a PC-controlled electrochemistry system (PAR, Model 273A). The $E_{1/2}$ value for the ferrocenium−ferrocene couple, under our experimental conditions, was 0.40 V. EPR spectra in the X-band were recorded with a JEOL Model JES-FA200 spectrometer. An elemental analyzer (Perkin−Elmer, Model 240C) was used to collect microanalytical data (C, H, N). ^1H NMR spectra were obtained using a spectrometer (Bruker, Model Avance DPX 300/400/500), and $SiMe_4$ was used as the internal standard. ESI mass spectra were recorded on a micro mass Q-TOF mass spectrometer (Serial No. YA 263).

Synthesis of $[(PPh_3)CpRu^{II}(L^3)Ru^{II}Cp(PPh_3)]Cl_2$ ($[\mathbf{1a}]Cl_2$). To a solution of 200 mg (0.28 mmol) $CpRu^{II}Cl(PPh_3)_2$ in 30 mL of methanol, 45 mg (0.32 mmol) 2-(methylthio)aniline, H_2L^1 was added and the mixture was stirred for 6 h. During this period, the color of the solution changed from yellow to dull green. The crude compound, obtained after evaporation of the solvent, was purified on a preparative alumina TLC plate. A chloroform−methanol solvent mixture was used

DOI: 10.1021/acs.inorgchem.5b00457
Inorg. Chem. 2015, 54, 6235−6244

as the eluent. A broad green zone was collected. Evaporation of the solvent yielded the compound $[(PPh_3)CpRu^{II}(L^3)Ru^{II}Cp(PPh_3)]Cl_2$ ($[\mathbf{1a}]Cl_2$). It was finally crystallized by slow evaporation of its solutions in a dichloromethane−methanol solvent mixture, which yielded a highly crystalline solid in 68% yield (110 mg). Anal. Calcd for $C_{60}H_{54}N_2P_2Ru_2S_2Cl_2$: C, 59.94; H, 4.53; N, 2.33. Found: C, 57.64; H, 4.70; N, 2.28. IR (KBr disk, cm^{-1}): 1635 (C═N). ESI-MS: m/z 566 for $([\mathbf{1a}]^{2+})/2$. ^1H NMR (500 MHz, CD_3OD): 8.55 (s, 1H, N−H), 7.73 (d, 1H, J = 13.5 Hz), 7.4−7.34 (m, 16H), 6.82 (s, 1H), 4.9 (s, 5H, Cp), 2.76 (s, 3H, CH_3).

Synthesis of $[(PPh_3)CpRu^{II}(L^4)Ru^{II}Cp(PPh_3)]Cl_2$ ($[\mathbf{1b}]Cl_2$). Complex $[\mathbf{1b}]Cl_2$ was prepared following a procedure identical to that described for $[\mathbf{1a}]Cl_2$ using 2-(phenylthio)aniline in place of 2-(methylthio)aniline. The isolated yields are characterization data are as follows:

Yield: (65%). Anal. Calcd for $C_{70}H_{58}N_2P_2Ru_2S_2Cl_2$: C, 63.39; H, 4.41; N, 2.11. Found: C, 62.64; H, 4.75; N, 2.06. IR (KBr disk, cm^{-1}): 1630 (C═N). ESI-MS: m/z 628 for $([\mathbf{1b}]^{2+})/2$. ^1H NMR (500 MHz, CD_3OD): 7.45−7.24 (m, 23H), 6.92 (s, 1H, N−H), 4.62 (s, 2H, Cp), 4.57 (s, 3H, Cp).

Synthesis of $[(PPh_3)CpRu^{II}(L^2)]Cl$ ($[\mathbf{2}]Cl$). A mixture of 100 mg (0.14 mmol) of $CpRu^{II}Cl(PPh_3)_2$ and 20 mg (0.16 mmol) of H_2L^2 in 50 mL of methanol was stirred for 4 h. The resulting brown solution was evaporated to dryness. The brown solid was purified on a preparative alumina TLC plate using chloroform/CH_3CN (4:1) as the eluent. A green brown band was isolated and recrystallized from by the slow diffusion of a dichloromethane solution of the compound into hexane. Yield: 72% (60 mg). The corresponding hexafluorophosphate salt, $[\mathbf{2}]PF_6$, was obtained in >90% yield by the addition of a saturated aqueous solution of $[NH_4]PF_6$ to a solution of $[\mathbf{2}]Cl$ in methanol. Anal. Calcd for $C_{29}H_{25}NP_2RuSF_6$: C, 50.00; H, 3.62; N, 2.01. Found: C, 50.05; H, 3.61; N, 2.04. IR (KBr disk, cm^{-1}): 1628 (C═N). ESI-MS: m/z 552 for $([\mathbf{2}]^+)$. ^1H NMR (500 MHz, $CDCl_3$): 15.35 (s, 1H, N−H), 7.47 (d, 1H, J = 9 Hz), 7.28−7.18 (m, 16H), 7.08 (t, 1H, J = 6.5 Hz), 6.80 (t, 1H, J = 8 Hz), 5.38 (s, 5H, Cp).

Computational Details. Full geometry optimizations were carried out using the density functional theory (DFT) method at the B3LYP.[25] All elements except ruthenium were assigned the 6-311G(d) basis set. The SDD basis set with effective core potential was employed for the Ru atom.[26] The vibrational frequency calculations were performed to ensure that the optimized geometries represent the local minima, and there are only positive Eigen values. All calculations were performed with Gaussian09 program package.[27] The broken-symmetry approach[28,29] was employed to establish the S = 0 state of compound $[\mathbf{1a}]^{2+}$. The calculation of the ground-state singlet was performed using spin-restricted or spin-unrestricted approaches (in Gaussian 09, combined with guess=mix). Stability analysis of the wave functions were performed using the "stable=opt" keyword. Mulliken spin densities were used for analysis of the spin populations on ligand and metal centers.[30] Vertical electronic excitations based on B3LYP optimized geometries were computed using the time-dependent density functional theory (TD-DFT) formalism[31] in acetonitrile using conductor-like polarizable continuum model (CPCM).[32] GaussSum[33] was used to calculate the fractional contributions of various groups to each molecular orbital.

Crystallography. Crystallographic data for the complexes $[\mathbf{1a}]Cl_2 \cdot 2H_2O$ and $[\mathbf{2}]PF_6$ are collected in Table 4. Suitable X-ray quality crystals of this compound are obtained by slow evaporation of its solution in a dichloromethane−methanol solvent mixture. The data were collected on a Bruker SMART APEX-II diffractometer, equipped with graphite-monochromated Mo Kα radiation (λ = 0.71073 Å), and was corrected for Lorentz-polarization effects. Unfortunately, the dataset for compound $[\mathbf{1a}]Cl_2 \cdot 2H_2O$ is incomplete, in terms of the range of 2θ used in the refinements; the molecular structure, nevertheless, present no unusual features and have been determined unambiguously. Our attempts to grow better crystals were unsuccessful.

$[\mathbf{1a}]Cl_2 \cdot 2H_2O$. A total of 25805 reflections were collected, 3957 of which were unique (R_{int} = 0.132), satisfying the ($I > 2\sigma(I)$) criterion, and were used in subsequent analysis.

Table 4. Crystallographic Data of the Complexes $[\mathbf{1a}]Cl_2 \cdot 2H_2O$ and $[\mathbf{2}]PF_6$

parameter	$[\mathbf{1a}]Cl_2 \cdot 2H_2O$	$[\mathbf{2}]PF_6$
empirical formula	$C_{60}H_{58}Cl_2N_2O_2P_2Ru_2S_2$	$C_{29}H_{25}NP_2RuSF_6$
formula weight	1238.20	696.58
temperature (K)	293	293
crystal system	monoclinic	monoclinic
space group	$P2_1/n$	$P2_1/n$
a (Å)	10.370(5)	9.373(5)
b (Å)	19.736(10)	18.972(5)
c (Å)	13.744(7)	15.682(5)
α (deg)	90	90
β (deg)	94.370(15)	101.537(5)
γ (deg)	90	90
V [Å^3]	2805(2)	2732.3(18)
Z	2	4
D_{calc} [g/cm^3]	1.466	1.693
crystal dimensions (mm^3)	0.09 × 0.12 × 0.14	0.08 × 0.11 × 0.15
θ range for data collection (deg)	1.8−23.2	1.7−27.5
GOF on F^2	1.05	1.03
reflections collected	25805	21387
unique reflections	3957	6136
final R indices [$I > 2\sigma(I)$]	$R1$ = 0.0555	$wR2$ = 0.1676
	$R1$ = 0.0554	$wR2$ = 0.1246

$[\mathbf{2}]PF_6$. A total of 21387 reflections were collected, 6136 of which were unique (R_{int} = 0.063), satisfying the ($I > 2\sigma(I)$) criterion, and were used in subsequent analysis.

The structure was solved by employing the SHELXS-97 program package[34a] and was refined by full-matrix least-squares based on F^2 (SHELXL-97).[34b]

The hydrogen atom (H1′) of imine group in the complexes $[\mathbf{1a}]Cl_2 \cdot 2H_2O$ and $[\mathbf{2}]PF_6$ is located from the electron density map, and the other hydrogen atoms were added in calculated positions.

■ ASSOCIATED CONTENT

Supporting Information

X-ray crystallographic file in CIF format for $[\mathbf{1a}]Cl_2 \cdot 2H_2O$ and $[\mathbf{2}]PF_6$; figures of ESI-MS and ^1H NMR spectra of $[\mathbf{1a}]Cl_2$, $[\mathbf{1b}]Cl_2$ and $[\mathbf{2}]PF_6$; cyclic voltammogram of $[\mathbf{1b}]Cl_2$; DFT results of $[\mathbf{1a}]^{2+}$, $[\mathbf{1b}]^{2+}$, and $[\mathbf{2}]^+$; coordinates of the DFT optimized structures are provided. The Supporting Information is available free of charge on the ACS Publications website at DOI: 10.1021/acs.inorgchem.5b00457.

■ AUTHOR INFORMATION

Corresponding Author

*E-mail: icsg@iacs.res.in.

Author Contributions

§P.G. and S.M. contributed equally to this work.

Notes

The authors declare no competing financial interest.

■ ACKNOWLEDGMENTS

Financial support received from the Department of Science and Technology (Project No. SR/S2/JCB-09/2011) and Council of Scientific and Industrial Research (Project No. 01(274)/13/EMR-II) New Delhi is gratefully acknowledged. S.G. thanks DST for a J.C. Bose fellowship. Crystallography was performed at the DST funded National Single Crystal Diffractometer Facility at the Department of Inorganic Chemistry, IACS. P.G.

DOI: 10.1021/acs.inorgchem.5b00457
Inorg. Chem. 2015, 54, 6235−6244

and I.C. thank the Council of Scientific and Industrial Research for fellowship support.

REFERENCES

(1) (a) Chirik, P. J.; Wieghardt, K. *Science* **2010**, *327*, 794−795. (b) Dzik, W. I.; van der Vlugt, J. I.; Reek, J. N. H.; de Bruin, B. *Angew. Chem., Int. Ed.* **2011**, *50*, 3356−3358. (c) Lyaskovskyy, V.; de Bruin, B. *ACS Catal.* **2012**, *2*, 270−279. (d) Grützmacher, H. *Angew. Chem., Int. Ed.* **2008**, *47*, 1814−1818. (e) Forum Issue on Redox Noninnocent Ligands: *Inorg. Chem.* **2011**, *50*, 9737.

(2) (a) Luca, O. R.; Crabtree, R. H. *Chem. Soc. Rev.* **2013**, *42*, 1440−1459. (b) Praneeth, V. K. K.; Ringenberg, M. R.; Ward, T. R. *Angew. Chem., Int. Ed.* **2012**, *51*, 10228−10234.

(3) (a) Jazdzewski, B. A.; Tolman, W. B. *Coord. Chem. Rev.* **2000**, *200−202*, 633−685. (b) Kaim, W. *Dalton Trans.* **2003**, 761−768. (c) Kaim, W.; Schwederski, B. *Coord. Chem. Rev.* **2010**, *254*, 1580−1588. (d) Chaudhuri, P.; Hess, M.; Flörke, U.; Wieghardt, K. *Angew. Chem., Int. Ed.* **1998**, *37*, 2217−2220. (e) Chaudhuri, P.; Hess, M.; Müller, J.; Hildenbrand, K.; Bill, E.; Weyhermüller, T.; Wieghardt, K. *J. Am. Chem. Soc.* **1999**, *121*, 9599−9610. (f) Mukherjee, C.; Pieper, U.; Bothe, E.; Bachler, V.; Bill, E.; Weyhermüller, T.; Chaudhuri, P. *Inorg. Chem.* **2008**, *47*, 8943−8956.

(4) (a) Kato, R. *Chem. Rev.* **2004**, *104*, 5319−5346. (b) Boyer, J. L.; Rochford, J.; Tsai, M.-K.; Muckerman, J. T.; Fujita, E. *Coord. Chem. Rev.* **2010**, *254*, 309−330.

(5) (a) Lever, A. B. P. *Coord. Chem. Rev.* **2010**, *254*, 1397−1405. (b) Metcalfe, R. A.; Lever, A. B. P. *Inorg. Chem.* **1997**, *36*, 4762−4771. (c) Metcalfe, R. A.; Dodsworth, E. S.; Fielder, S. S.; Stufkens, D. J.; Lever, A. B. P.; Pietro, W. J. *Inorg. Chem.* **1996**, *35*, 7741−7750.

(6) (a) Eisenberg, R.; Gray, H. B. *Inorg. Chem.* **2011**, *50*, 9741−9751. (b) Ray, K.; Petrenko, T.; Wieghardt, K.; Neese, F. *Dalton Trans.* **2007**, 1552−1566. (c) Sugimoto, H.; Tsukube, H. *Chem. Soc. Rev.* **2008**, *37*, 2609−2619.

(7) (a) Poddel'sky, A. I.; Cherkasov, V. K.; Abakumov, G. A. *Coord. Chem. Rev.* **2009**, *253*, 291−324. (b) Chun, H.; Verani, C. N.; Chaudhuri, P.; Bothe, E.; Bill, E.; Weyhermüller, T.; Wieghardt, K. *Inorg. Chem.* **2001**, *40*, 4157−4166. (c) Kokatam, S.; Weyhermüller, T.; Bothe, E.; Chaudhuri, P.; Wieghardt, K. *Inorg. Chem.* **2005**, *44*, 3709−3717. (d) Chun, H.; Bill, E.; Bothe, E.; Weyhermüller, T.; Wieghardt, K. *Inorg. Chem.* **2002**, *41*, 5091−5099. (e) Sun, X.; Chun, H.; Hildenbrand, K.; Bothe, E.; Weyhermüller, T.; Neese, F.; Wieghardt, K. *Inorg. Chem.* **2002**, *41*, 4295−4303. (f) Das, D.; Sarkar, B.; Mondal, T. K.; Mobin, S. M.; Fiedler, J.; Kaim, W.; Lahiri, G. K. *Inorg. Chem.* **2011**, *50*, 7090−7098.

(8) (a) Verani, C. N.; Gallert, S.; Bill, E.; Weyhermüller, T.; Wieghardt, K.; Chaudhuri, P. *Chem. Commun.* **1999**, 1747−1748. (b) Herebian, D.; Bothe, E.; Bill, E.; Weyhermüller, T.; Wieghardt, K. *J. Am. Chem. Soc.* **2001**, *123*, 10012−10023. (c) Ghosh, P.; Bill, E.; Weyhermüller, T.; Wieghardt, K. *J. Am. Chem. Soc.* **2003**, *125*, 3967−3979. (d) Ghosh, P.; Begum, A.; Bill, E.; Weyhermüller, T.; Wieghardt, K. *Inorg. Chem.* **2003**, *42*, 3208−3215. (e) Ebadi, M.; Lever, A. B. P. *Inorg. Chem.* **1999**, *38*, 467−474. (h) Patra, S.; Sarkar, B.; Mobin, S. M.; Kaim, W.; Lahiri, G. K. *Inorg. Chem.* **2003**, *42*, 6469−6473.

(9) (a) Butin, K. P.; Beloglazkina, E. K.; Zyk, N. V. *Russ. Chem. Rev.* **2005**, *74*, 531−553. (b) Sproules, S.; Wieghardt, K. *Coord. Chem. Rev.* **2010**, *254*, 1358−1382. (c) Ward, M. D.; McCleverty, J. A. *J. Chem. Soc., Dalton Trans.* **2002**, 275−288.

(10) (a) Schweinfurth, D.; Das, H. S.; Weisser, F.; Bubrin, D.; Sarkar, B. *Inorg. Chem.* **2011**, *50*, 1150−1159. (b) Hübner, R.; Weber, S.; Strobel, S.; Sarkar, B.; Záliš, S.; Kaim, W. *Organometallics* **2011**, *30*, 1414−1418.

(11) Chatterjee, S.; Mandal, S.; Samanta, S.; Goswami, S. *Dalton Trans.* **2012**, *41*, 7057−7066.

(12) Mandal, S.; Samanta, S.; Mondal, T. K.; Goswami, S. *Organometallics* **2012**, *31*, 5282−5293.

(13) Plane 1 defined by C2-C3-C4-C5-C6 and plane 2 defined by C2_a-C3_a-C4_a-C5_a-C6_a.

(14) (a) Jüstel, T.; Bendix, J.; Metzler-Nolte, N.; Weyhermüller, T.; Nuber, B.; Wieghardt, K. *Inorg. Chem.* **1998**, *37*, 35−43. (b) Rusanova, J.; Rusanov, E.; Gorelsky, S. I.; Christendat, D.; Popescu, R.; Farah, A. A.; Beaulac, R.; Reber, C.; Lever, A. B. P. *Inorg. Chem.* **2006**, *45*, 6246−6262.

(15) Conner, D.; Jayaprakash, K. N.; Gunnoe, T. B.; Boyle, P. D. *Organometallics* **2002**, *21*, 5265−5271 and reference therein..

(16) (a) Conner, D.; Jayaprakash, K. N.; Gunnoe, T. B.; Boyle, P. D. *Inorg. Chem.* **2002**, *41*, 3042−3049. (b) Jayaprakash, K. N.; Gunnoe, T. B.; Boyle, P. B. *Inorg. Chem.* **2001**, *40*, 6481−6486. (c) Takemoto, S.; Yamazaki, Y.; Yamano, T.; Mashima, D.; Matsuzaka, H. *J. Am. Chem. Soc.* **2012**, *134*, 17027−17035. (d) Nakajima, Y.; Sakaki, S.; Nakao, Y.; Suzuki, H. *Organometallics* **2012**, *31*, 5342−5348. (e) Ohkuma, T.; Utsumi, N.; Tsutsumi, K.; Murata, K.; Sandoval, C.; Noyori, R. *J. Am. Chem. Soc.* **2006**, *128*, 8724−8725.

(17) (a) Mandal, S.; Paul, N.; Banerjee, P.; Mondal, T. K.; Goswami, S. *Dalton Trans.* **2010**, *39*, 2717−2726. (b) Mandal, S.; Castiñeiras, A.; Mondal, T. K.; Mondal, A.; Chattopadhyay, D.; Goswami, S. *Dalton Trans.* **2010**, *39*, 9514−9522.

(18) (a) Metcalfe, R. A.; Dodsworth, E. S.; Lever, A. B. P.; Pietro, W. J.; Stufkens, D. J. *Inorg. Chem.* **1993**, *32*, 3581−3582. (b) Hartl, F.; Snoeck, T. L.; Stufkens, D. J.; Lever, A. B. P. *Inorg. Chem.* **1995**, *34*, 3887−3894. (c) Metcalfe, R. A.; Dodsworth, E. S.; Fielder, S. S.; Stufkens, D. J.; Lever, A. B. P.; Pietro, W. J. *Inorg. Chem.* **1996**, *35*, 7741−7750. (d) Kaim, W.; Lahiri, G. K. *Angew. Chem., Int. Ed.* **2007**, *46*, 1778−1796. (e) Barthram, A. M.; Ward, M. D. *New J. Chem.* **2000**, *24*, 501−504. (f) Metcalfe, R. A.; Vasconcellos; Luiz, C. G.; Mirza, H.; Franco, D. W.; Lever, A. B. P. *J. Chem. Soc., Dalton Trans.* **1999**, 2653−2667. (g) Haga, M.; Ali, M. M.; Koseki, S.; Fujimoto, K.; Yoshimura, A.; Nozaki, K.; Ohno, T.; Nakajima, K.; Stufkens, D. J. *Inorg. Chem.* **1996**, *35*, 3335−3347. (h) Ghumaan, S.; Sarkar, B.; Maji, S.; Puranik, V. G.; Fiedler, J.; Urbanos, F. A.; Jimenez-Aparicio, R.; Kaim, W.; Lahiri, G. K. *Chem.—Eur. J.* **2008**, *14*, 10816−10828. (i) Patra, S.; Sarkar, B.; Ghumaan, S.; Fiedler, J.; Záliš, S.; Kaim, W.; Lahiri, G. K. *Dalton Trans.* **2004**, 750−753.

(19) Cini, R.; Bozzi, R.; Karaulov, A.; Hursthouse, M. B.; Calafat, A. M.; Marzilli, L. G. *J. Chem. Soc., Chem. Commun.* **1993**, 899−901.

(20) Poater, J.; Sol, M.; Bickelhaupt, F. M. *Chem.—Eur. J.* **2006**, *12*, 2889−2895.

(21) (a) Dugan, T. R.; Bill, E.; MacLeod, K. C.; Christian, G. J.; Cowley, R. E.; Brennessel, W. W.; Ye, S.; Neese, F.; Holland, P. L. *J. Am. Chem. Soc.* **2012**, *134*, 20352−20364. (b) Lewis, R. A.; MacLeod, K. C.; Mercado, B. Q.; Holland, P. L. *Chem. Commun.* **2014**, *50*, 11114−11117.

(22) (a) Chelucci, G.; Thummel, R. P. *Chem. Rev.* **2002**, *102*, 3129−3170. (b) Steenwinkel, P.; Grove, D. M.; Veldman, N.; Spek, A. L.; Koten, G. V. *Organometallics* **1998**, *17*, 5647−5655.

(23) Bruce, M. I.; Hameister, C.; Swincer, A. G.; Wallis, R. C. *Inorg. Synth.* **1990**, *28*, 270−272.

(24) Goswami, S.; Mukherjee, R. N.; Chakravarty, A. *Inorg. Chem.* **1983**, *22*, 2825−2832.

(25) (a) Becke, A. D. *J. Chem. Phys.* **1993**, *98*, 5648−5652. (b) Lee, C.; Yang, W.; Parr, R. G. *Phys. Rev. B: Condens. Matter Mater. Phys.* **1988**, *37*, 785−789. (c) Vosko, S. H.; Wilk, L.; Nusair, M. *Can. J. Phys.* **1980**, *58*, 1200−1211. (d) Stephens, P. J.; Devlin, F. J.; Chabalowski, C. F.; Frisch, M. J. *J. Phys. Chem.* **1994**, *98*, 11623−11627.

(26) (a) Andrae, D.; Haeussermann, U.; Dolg, M.; Stoll, H.; Preuss, H. *Theor. Chim. Acta* **1990**, *77*, 123−141. (b) Fuentealba, P.; Preuss, H.; Stoll, H.; Szentpaly, L. V. *Chem. Phys. Lett.* **1982**, *89*, 418−422.

(27) Frisch, M. J.; Trucks, G. W.; Schlegel, H. B.; Scuseria, G. E.; Robb, M. A.; Cheeseman, J. R.; Montgomery, Jr., J. A.; Vreven, T.; Kudin, K. N.; Burant, J. C.; Millam, J. M.; Iyengar, S. S.; Tomasi, J.; Barone, V.; Mennucci, B.; Cossi, M.; Scalmani, G.; Rega, N.; Petersson, G. A.; Nakatsuji, H.; Hada, M.; Ehara, M.; Toyota, K.; Fukuda, R.; Hasegawa, J.; Ishida, M.; Nakajima, T.; Honda, Y.; Kitao, O.; Nakai, H.; Klene, M.; Li, X.; Knox, J. E.; Hratchian, H. P.; Cross, J. B.; Bakken, V.; Adamo, C.; Jaramillo, J.; Gomperts, R.; Stratmann, R. E.; Yazyev, O.; Austin, A. J.; Cammi, R.; Pomelli, C.; Ochterski, J. W.; Ayala, P. Y.; Morokuma, K.; Voth, G. A.; Salvador, P.; Dannenberg, J. J.; Zakrzewski, V. G.; Dapprich, S.; Daniels, A. D.; Strain, M. C.; Farkas, O.; Malick, D. K.; Rabuck, A. D.; Raghavachari, K.; Foresman,

DOI: 10.1021/acs.inorgchem.5b00457
Inorg. Chem. 2015, 54, 6235−6244

J. B.; Ortiz, J. V.; Cui, Q.; Baboul, A. G.; Clifford, S.; Cioslowski, J.; Stefanov, B. B.; Liu, G.; Liashenko, A.; Piskorz, P.; Komaromi, I.; Martin, R. L.; Fox, D. J.; Keith, T.; Al-Laham, M. A.; Peng, C. Y.; Nanayakkara, A.; Challacombe, M.; Gill, P. M. W.; Johnson, B.; Chen, W.; Wong, M. W.; Gonzalez, C.; Pople, J. A. *Gaussian 09, Revision C.01*; Gaussian, Inc.: Wallingford, CT, 2010.

(28) Ginsberg, A. P. *J. Am. Chem. Soc.* **1980**, *102*, 111−117.

(29) (a) Noodleman, L.; Case, D. A.; Aizman, A. *J. Am. Chem. Soc.* **1988**, *110*, 1001−1005. (b) Noodleman, L.; Davidson, E. R. *Chem. Phys.* **1986**, *109*, 131−143. (c) Noodleman, L.; Norman, J. G., Jr.; Osborne, J. H.; Aizman, C.; Case, D. A. *J. Am. Chem. Soc.* **1985**, *107*, 3418−3426. (d) Noodleman, L. *J. Chem. Phys.* **1981**, *74*, 5737−5743.

(30) Mulliken, R. S. *J. Chem. Phys.* **1955**, *23*, 1833−1840.

(31) (a) Bauernschmitt, R.; Ahlrichs, R. *Chem. Phys. Lett.* **1996**, *256*, 454−464. (b) Stratmann, R. E.; Scuseria, G. E.; Frisch, M. J. *J. Chem. Phys.* **1998**, *109*, 8218−8224. (c) Casida, M. E.; Jamoroski, C.; Casida, K. C.; Salahub, D. R. *J. Chem. Phys.* **1998**, *108*, 4439−4449.

(32) (a) Cossi, M.; Rega, N.; Scalmani, G.; Barone, V. *J. Comput. Chem.* **2003**, *24*, 669−681. (b) Cossi, M.; Barone, V. *J. Chem. Phys.* **2001**, *115*, 4708−4717. (c) Barone, V.; Cossi, M. *J. Phys. Chem. A* **1998**, *102*, 1995−2001. (d) O'Boyle, N. M.; Tenderholt, A. L.; Langner, K. M. *J. Comput. Chem.* **2008**, *29*, 839−845.

(33) Leininger, T.; Nicklass, A.; Stoll, H.; Dolg, M.; Schwerdtfeger, P. J. *J. Chem. Phys.* **1996**, *105*, 1052−1059.

(34) (a) Sheldrick, G. M. *Acta Crystallogr., Sect. A: Found. Crystallogr.* **1990**, *46*, 467−473. (b) Sheldrick, G. M. *SHELXL 97, Program for the Refinement of Crystal Structures*; University of Göttingen: Göttingen, Germany, 1997.

DOI: 10.1021/acs.inorgchem.5b00457
Inorg. Chem. 2015, 54, 6235−6244